IEEE Photonics Journal
An IEEE Photonics Society Publication

Open Access

Photonic Generation of Microwave Signals Using a Single-Mode VCSEL Subject to Dual-Beam Orthogonal Optical Injection

Volume 7, Number 1, February 2015

Pablo Pérez
Ana Quirce
Angel Valle
Antonio Consoli
Ignacio Noriega
Luis Pesquera
Ignacio Esquivias

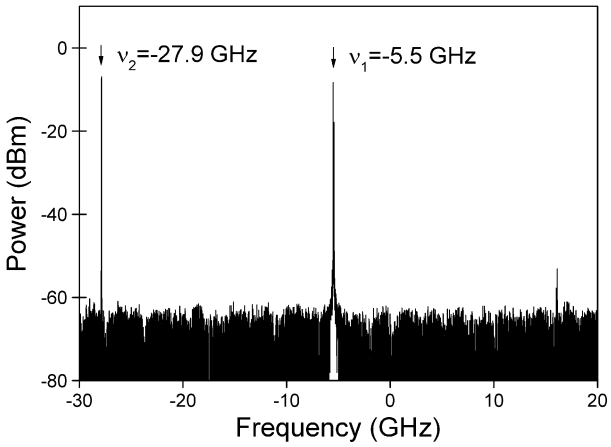

DOI: 10.1109/JPHOT.2015.2400391
1943-0655 © 2015 IEEE

IEEE photonics SOCIETY

IEEE

Photonic Generation of Microwave Signals Using a Single-Mode VCSEL Subject to Dual-Beam Orthogonal Optical Injection

Pablo Pérez,[1,4] Ana Quirce,[2] Angel Valle,[1] Antonio Consoli,[3] Ignacio Noriega,[1] Luis Pesquera,[1] and Ignacio Esquivias[3]

[1]Instituto de Física de Cantabria, CSIC-Universidad de Cantabria, 39005 Santander, Spain
[2]Brussels Photonics Team, Department of Applied Physics and Photonics, (B-PHOT TONA) Vrije Universiteit Brussel, 1050 Brussels, Belgium
[3]CEMDATIC-ETSI de Telecomunicación, Universidad Politécnica de Madrid, 28040 Madrid, Spain
[4]Departamento de Física Moderna, Universidad de Cantabria, 39005 Santander, Spain

DOI: 10.1109/JPHOT.2015.2400391

Manuscript received January 8, 2015; revised January 30, 2015; accepted January 30, 2015. Date of publication February 5, 2015; date of current version February 19, 2015. This work was supported in part by the Ministerio de Economía y Competitividad, Spain, under Project TEC2012-38864-C03-02 and Project TEC2012-38864-C03-03 and in part by FEDER funds. Corresponding author: A. Valle (e-mail: valle@ifca.unican.es).

Abstract: We experimentally and theoretically investigate the photonic generation of microwave signals using a long-wavelength single-transverse-mode vertical-cavity surface-emitting laser (VCSEL) subject to two-frequency orthogonal optical injection. We study if a significant reduction of the linewidth is achieved in the double injection locking regime. In this regime, the VCSEL is subject to optical injection by two master lasers in such a way that stable locking is also observed if only light from one of the master lasers is injected. Our model includes the effect of the injected light reflected at the VCSEL's mirror generalizing previous modeling of reflection-mode optical injection-locked VCSELs. Our model also describes the high coherence associated to stable injection locking states and takes into account phase fluctuations in both master lasers. We observe no significant reduction of the linewidth in the double injection locking regime because the linewidth is mainly determined by the phase fluctuations of the two master lasers.

Index Terms: Semiconductor lasers, vertical-cavity surface-emitting laser (VCSEL), optical injection, photonic microwave generation, radio-over-fiber (RoF), nonlinear dynamics.

1. Introduction

Semiconductor lasers exhibit a rich variety of nonlinear dynamical behaviors and are of interest from a fundamental and from an application point of view [1]. A usual way of obtaining these behaviors is by injecting laser light in the semiconductor laser. This technique can be used for reducing the laser linewidth, the mode partition noise or for enhancing the modulation bandwidth without modifying the semiconductor laser design [2]. One of the applications of the optical injection in semiconductor lasers that has attracted a great interest is the photonic microwave generation.

Photonic microwave sources producing highly stable and broadly tunable microwave frequencies are interesting for applications ranging from broadband wireless access networks to photonic microwave signal processing [3]–[6]. Microwave signal generation using photonics has the

advantages of high speed, low power consumption, low cost, and high reliability [3]–[6]. Large values of the propagation losses of high-frequency microwaves in free space make the optical fiber a good choice to transmit an optical carrier that carries the microwave signal with large bandwidth and low loss over long distances. Different photonic microwave generation techniques include direct modulation of semiconductor lasers, optical mixing or optical heterodyning, external modulation using Mach–Zehnder modulators, mode-locked semiconductor lasers, and optical injection locking in semiconductor lasers [4]. In the optical mixing scheme, two optical waves detuned at a desired frequency beat directly at a photodetector to generate the microwave beat signal. The beat signal has large phase noise if the two optical beams are not phase correlated. Optical injection locking can be used to generate a high-quality microwave signal because the phase terms of the two optical waves used for heterodyning are highly correlated [7]. Also, optical phase lock loops (OPLLs) have demonstrated optical beams with locked phases, and, hence, RF signals with high spectral purity [4]. However optical injection locking and OPLLs need a microwave reference source for phase stabilization and sideband generation which significantly increases the cost and complexity of the system [6]. Also, dual-wavelength fiber lasers can be used to increase phase correlation between two lasing wavelengths because they share the same laser cavity [6]. Dual-wavelength fiber lasers can be obtained by using a filter in the laser cavity to select the lasing modes. In these systems, frequency tuning is achieved through meticulous mechanical or thermal adjustments [6].

Photonic microwave generation techniques based on the period-one (P1) nonlinear dynamics of optically injected semiconductor lasers have also attracted a lot of interest [6], [8]–[18]. This approach allows widely tunable, optically controlled and single sideband generation of microwave signals [6]. P1 oscillation can be viewed as the beating of two dominant wavelengths: one is regenerated from the optical injection while the other is emitted near the cavity resonance wavelength [10]. The generated frequency range far exceeds the intrinsic relaxation oscillation frequency of the semiconductor laser. Photonic microwaves based on P1 dynamics have reached frequency values beyond 100 GHz [11] with a tuning range that is limited to several tens of GHz [8]. The generated microwave has a relatively large linewidth on the order of a few megahertz. A double-lock technique using a stable electronic microwave source [12] has been used to obtain a RF linewidth below 1 kHz. Generation of microwave signals with simultaneous high frequency and low phase noise have been obtained by using the P1 dynamics of optically injected semiconductor lasers subject to optical feedback [9], [13], [16].

Very recently, microwave generation using dual-beam optical injection in semiconductor lasers has also been investigated [8], [18]–[23]. Microwave signals with frequencies corresponding to the frequency difference between the master lasers can be generated [8]. This optical injection scheme does not require a microwave reference source. It has also the advantages of low system complexity, narrow linewidth, low cost, single sideband generation, small power fluctuations, and a much broader tuning range than the single-beam injection scheme [8], [18]. A very high frequency (121.7 GHz) microwave signal has been generated by using a dual-beam optically injected single-mode DFB laser [8]. “Double injection locking” (DIL) is observed when the slave laser is subject to strong optical injection by both master lasers in such a way that stable locking is also observed if only light from one of the master lasers is injected [8], [18]. Comparison of the performance with a similar P1 oscillation signal generated with single optical injection shows that a significant reduction of the linewidth is achieved when using the DIL scheme due to the phase-locking and high coherence associated to stable injection locking states [18].

Photonic microwave generation using vertical-cavity surface-emitting lasers (VCSELs) instead of a DFB laser subject to dual-beam optical injection has also been recently considered in a theoretical way [22], [23]. VCSELs have inherent advantages in comparison with edge-emitting devices. These advantages include single-longitudinal mode operation, circular beam profile, low threshold current, reduced fabrication costs, and ease of fabrication of 2-D arrays [24], [25]. These devices also have additional degrees of freedom when compared to their edge emitting counterparts like the direction of the emitted polarization or the possibility of emission in multiple transverse modes that can enhance microwave generation [22]. Many of the studies of VCSELs

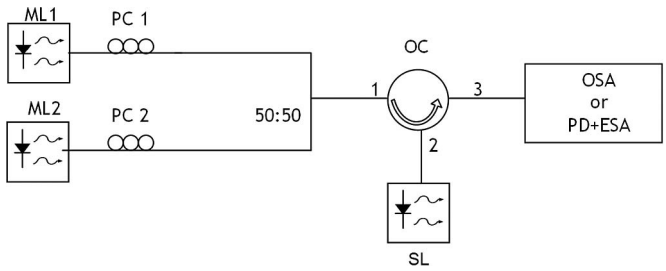

Fig. 1. Experimental setup for orthogonal optical injection into a VCSEL. ML: master laser, PC: polarization controller, OC: optical circulator, SL: slave laser, OSA: optical spectrum analyzer, ESA: electrical spectrum analyzer.

subject to optical injection consider the so-called “orthogonal optical injection” [26]–[28]. In this configuration, linearly polarized light from an external laser is injected orthogonally to the linear polarization of a free-running VCSEL [26]. This is also the kind of injection considered in [23].

In this work we experimentally and theoretically investigate the photonic generation of microwave signals using a long-wavelength single transverse mode VCSEL subject to dual-beam orthogonal optical injection. We use this configuration because it corresponds to a situation that has not been addressed previously in experiments in order to study the characteristics of the generated microwave signals. One of the motivations of this work is the understanding of microwave generation in a single-mode VCSEL as a first step in the analysis of the enhanced microwave generation found in the theoretical study of the more complicated multi-mode VCSELs [22], [23]. We study the underlying dual injection locking VCSEL dynamics. We focus on the transition to the DIL regime. We prefer to use the terminology of [8] “double injection locking” despite the fact that no stationary state exists when such a “locking” is achieved—a beat note at the frequency difference of the two master lasers exists- because it incorporates well the fact that stable locking is observed for both master lasers individually. We theoretically analyze if a significant reduction of the linewidth is achieved in the DIL regime. Our model consists on a set of rate equations with optical injection that takes into account phase fluctuations in both master lasers and that describes the coherence phenomena associated to stable injection locking states. We compare our experimental results with simulations of a model using the parameters extracted for the VCSEL of our experiment [29], [30]. Our model also includes the effect of the injected light reflected at the VCSEL's mirror because the experiment is performed in the reflection-mode. Our equations extend the theoretical modelling of reflection-mode optical injection-locked VCSELs [31], [32] since a variety of dynamical states, which are not restricted to injection locking, can be analyzed. The good agreement found between theory and experiment permits us to perform a theoretical analysis in which we do not observe a significant reduction of the linewidth in the DIL regime because the linewidth is mainly determined by the phase fluctuations of the two master lasers. The corresponding discussion on the relation between the optical phase of the VCSEL and those of both master lasers is included at the end of our work.

The paper is organized as follows. In Section 2, we describe the experimental setup. Section 3 describes the theoretical model. In Section 4, we present our theoretical and experimental results. In Section 5 a discussion of our results is presented, and finally, in Section 6, we summarize our results.

2. Experimental Set-Up

Dual-beam orthogonal optical injection in a long-wavelength VCSEL is obtained by using the all-fiber experimental set up shown in Fig. 1. It includes two Master Lasers (ML1, ML2) and a VCSEL slave laser (SL). This is a single-transverse mode device (Raycan RC331-FFA pigtail VCSEL) emitting in the 1550 nm wavelength region. ML1 is another similar single-transverse mode VCSEL and ML2 is a tunable external cavity laser (Tunics Plus CL). Both VCSELs were temperature controlled with a thermo electric cooler and all measurements were performed at a

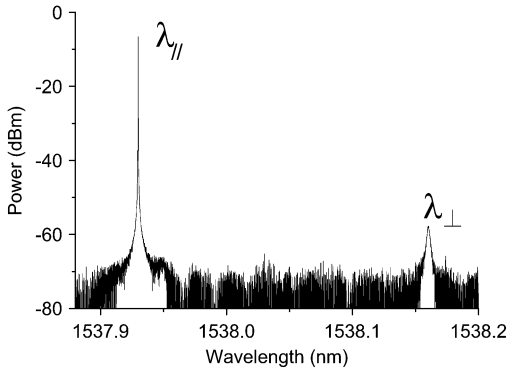

Fig. 2. Optical spectrum of the solitary VCSEL biased with a current of 4 mA.

constant temperature of 25 °C. Polarization Controllers (PC) were used for each master laser in order to inject light with a linear polarization orthogonal to that of the free-running slave VCSEL. Control of the injected light polarization is carried out separately for each master laser. The VCSELs used in these experiments have threshold currents around 1.6 mA and show Polarization Switching (PS) between stable linear polarization states oriented in orthogonal directions (that we will call "parallel" and "orthogonal") when the bias current is increased, at a bias current of 6 mA. In our experiments, the driving currents of both VCSELs have been chosen in order to emit in a stable linear polarization state. The slave VCSEL is biased at $I = 4$ mA, and it emits in the parallel linear polarization with a power of 320 μW and with a relaxation oscillation frequency of 2.8 GHz.

We show in Fig. 2 the corresponding optical spectrum. Optical spectrum has been measured with a 10 MHz resolution bandwidth. The wavelength of the parallel (orthogonal) polarization is $\lambda_{\parallel} = 1537.93$ nm ($\lambda_{\perp} = 1538.17$ nm). These linear polarization modes are spaced 0.24 nm (30 GHz). Higher-order transverse modes do not play any role in our experiment because they are suppressed more than 55 dB at 4 mA bias current. Light from both MLs is sent to the input ports of a 50 : 50 fiber coupler and injected into the VCSEL through an Optical Circulator (OC). The signal at port 3 of the OC entered a 50:50 fiber coupler and was sent to the high-resolution Brillouin Optical Spectrum Analyzer (BOSA, Aragon Photonics, with 10 MHz bandwidth resolution) and to a 9.5 GHz bandwidth photodiode (PD, Thorlabs PDA8GS) connected to an Electrical Spectrum Analyzer (ESA, Anritsu MS2719B, 9 kHz–20 GHz). Note that in addition to the VCSEL's output, the signal analyzed at OSA or ESA also includes the reflection of the optical injection from the front surface of the VCSEL.

3. The Model

We theoretically study the dynamics of the polarization of the VCSEL with the widely used spin-flip model (SFM) [33] in which we have added two optical injection terms in the equation for the e-field of one of the linear polarizations. The model equations are given by (1)–(4), shown below, where $E_{x,y}$ are the two linearly polarized slowly varying components of the (scaled) field and D and n are two (scaled) carrier variables. D accounts for the total population inversion between conduction and valence bands, while n is the difference between the population inversions for the spin-up and spin-down radiation channels. In order to consider a more realistic calculation of the RF linewidths of the generated signals we have also taken into account finite linewidths of the optical spectrum of both master lasers. Therefore, we consider the variable $\phi_i (i = 1, 2)$ that is the random phase of the i-ML. In previous works [29], [30], we have obtained the values of the parameters of the model that characterize the VCSEL used as SL in this work. The scaled total population inversion is given by $D = G_N(N - N_t)/(2\kappa)$, where $G_N = 2.152 \cdot 10^4$ s^{-1} is the differential gain, $\kappa = 33$ ns^{-1} is the field decay rate and N and N_t are the number of carriers in the active region and at transparency, respectively. The same scaling factor is

used for n. The rest of internal VCSEL parameters are as follows: $\alpha = 2.8$ is the linewidth enhancement factor, μ is a normalized bias current, $\gamma_s = 2100$ ns^{-1} is the spin-flip relaxation rate, $\gamma_a = 0.3$ ns^{-1} is the linear dichroism, $\gamma = 2.08$ ns^{-1} is the decay rate of D, and $\gamma_p = 95.19$ ns^{-1} is the linear birefringence

$$\frac{dE_x}{dt} = -(\kappa+\gamma_a)E_x - i(\kappa\alpha+\gamma_p)E_x + \kappa(1+i\alpha)(DE_x + inE_y) + \kappa E_{inj,1}e^{i(\Delta\omega_1 t+\phi_1(t))} + \kappa E_{inj,2}e^{i(\Delta\omega_2 t+\phi_2(t))} + \sqrt{\frac{R_+}{2}}\xi_+(t) + \sqrt{\frac{R_-}{2}}\xi_-(t) \quad (1)$$

$$\frac{dE_y}{dt} = -(\kappa-\gamma_a)E_y - i(\kappa\alpha-\gamma_p)E_y + \kappa(1+i\alpha)(DE_y - inE_x) + i\left(\sqrt{\frac{R_+}{2}}\xi_-(t) - \sqrt{\frac{R_-}{2}}\xi_+(t)\right) \quad (2)$$

$$\frac{dD}{dt} = -\gamma\left[D\left(1+|E_x|^2+|E_y|^2\right) - \mu + in\left(E_yE_x^* - E_xE_y^*\right)\right] \quad (3)$$

$$\frac{dn}{dt} = -\gamma_s n - \gamma\left[n\left(|E_x|^2+|E_y|^2\right) + iD\left(E_yE_x^* - E_xE_y^*\right)\right] \quad (4)$$

$$\frac{d\phi_1}{dt} = \xi_1(t) \quad (5)$$

$$\frac{d\phi_2}{dt} = \xi_2(t). \quad (6)$$

The scaled spontaneous emission rates are given by $R_\pm = \beta_{SF}\gamma[(D \pm n) + G_N N_t/(2\kappa)]$, where β_{SF} accounts for the fraction of spontaneously emitted photons that are coupled into the laser mode. Fluctuations due to spontaneous emission in the slave VCSEL are included in our calculations by $\xi_+(t)$ and $\xi_-(t)$ (complex Gaussian noise terms of zero mean and time correlation given by $\langle \xi_i(t)\xi_j^*(t')\rangle = \delta_{ij}\delta(t-t'))$. In our case, $\beta_{SF} = 6.5\cdot 10^{-4}$. Independent real Gaussian noise terms, $\xi_1(t)$ and $\xi_2(t)$, of zero mean and time correlation given by $\langle \xi_i(t)\xi_i(t')\rangle = 2\beta_i\delta(t-t')$, $i = 1,2$ are considered to obtain the phase diffusion of the i-ML due to its spontaneous emission. The phase of the i-ML, $\phi_i(t)$, is a random variable so that the resulting frequency spectrum of the external field with just phase-fluctuation has a Lorentzian lineshape with a linewidth of β_i/π [34]. The pump parameter μ is related to the bias current I, (fixed in this work, I = 4 mA), the threshold current ($I_{th} = 1.602$ mA), the number of carriers at transparency ($N_t = 9\cdot 10^6$), the number of carriers at threshold ($N_{th} = 1.21\cdot 10^7$), the differential carrier lifetime at threshold ($\tau_e = 1.21$ ns) and the carrier lifetime at threshold ($\tau_n = 0.48$ ns) by the following expression [30]:

$$\mu = \frac{\tau_n}{\tau_e}\frac{\frac{I}{I_{th}} - 1}{1 - \frac{N_t}{N_{th}}} + 1. \quad (7)$$

The parameter values correspond to a VCSEL that emits in the y or "parallel" linear polarization. The subsidiary x or "orthogonal" polarization mode is shifted 0.24 nm to the long wavelength side of the lasing mode, as in our device. In this way the angular frequency of the parallel polarized mode, ω_y, is larger than that of the orthogonal linear polarization, ω_x. Optical injection is included in the model by considering the parameters $E_{inj,1}$, $E_{inj,2}$, $\Delta\omega_1$, and $\Delta\omega_2$. $E_{inj,1}$ and $E_{inj,2}$ are the amplitudes of the injected fields by ML1 and ML2, respectively, in the orthogonal polarization. $\Delta\omega_i (i = 1,2)$ is defined as the difference between the angular frequency of the light emitted by the i-ML, $\omega_{inj,i}$, and a reference angular frequency intermediate between those of the x and y linear polarizations, i.e., $\Delta\omega_i = \omega_{inj,i} - (\omega_x+\omega_y)/2$, where $\omega_x = -\gamma_p + \alpha\gamma_a$, and $\omega_y = \gamma_p - \alpha\gamma_a$. In this paper results will be given in terms of two frequency detunings, ν_1 and ν_2, where ν_i is the frequency detuning between the i-ML frequency and the frequency of the orthogonal polarization, ($\nu_i = \nu_{inj,i} - \nu_x$). Our choice of the strength of the input coupling is the same than that used in [33]. The input coupling coefficient coincides with κ for the ideal case of an effectively mode-matched injected input beam [33].

The observed signal in our experiments is the coherent addition of two signals: the VCSEL emission and the reflection of both optical injections from the front surface of the VCSEL. We can obtain the observed e-field from our model, $\vec{E}_{obs}(t)$, by considering that the phase shift of the optical injection after the reflection at the VCSEL's DBR is around π [31]:

$$\vec{E}_{obs} = E_x(t)\vec{i} + E_y(t)\vec{j} - \eta\sqrt{R}\left(E_{inj,1}e^{j(\Delta\omega_1 t+\varphi_1(t))} + E_{inj,2}e^{j(\Delta\omega_2 t+\varphi_2(t))}\right)\vec{i} \quad (8)$$

where R is the power reflectance of the DBR ($R = 0.995$), and $\vec{i}$ and $\vec{j}$ are the unitary vectors in the orthogonal and parallel directions, respectively. In (8), we introduce an injection efficiency factor, η, that takes into account the fact that the light from MLs that is going to be reflected at the VCSEL has more losses than the light emitted by the VCSEL. The VCSEL light is coupled into a fiber by a spherical lens in an efficient manner. However, the light from MLs leaves the fiber within the acceptance cone determined by the fiber, part of it is focused by that spherical lens, reflected in the VCSEL and focused again in the fiber by the lens. This process is much less efficient than the coupling of VCSEL light in the fiber. Our equations extend the theoretical modelling of reflection-mode optical injection-locked VCSELs [31], [32] not only because of the presence of a second optical injection but since a variety of dynamical states, which not restricted to injection locking, can be analyzed as well.

4. Results

In the experiment, the strength of the optical injection is given by the injected powers from ML1 and ML2 measured in port 2 of the circulator, $P_{ML1} = 108\ \mu W$ and $P_{ML2} = 865\ \mu W$, respectively. These values remain fixed during the experiment. In our first set of measurements the frequency of ML1 ($\nu_1 = -5.5$ GHz) is kept fixed while the frequency of the tunable laser ML2, i.e., ν_2, is changed. P_{ML1} and ν_1 are such that there is polarization switching (PS) under single optical injection. This PS is such that the VCSEL is locked to the optical injection. We note that when the VCSEL is subject to single optical injection PS and locking regions coincide when the frequency detuning with respect to the orthogonal polarization is negative [35]. Fig. 3 shows the dynamics obtained when the frequency of ML2 is smaller than that of ML1, $\nu_2 < \nu_1$. The left column of Fig. 3 shows the experimental optical spectra of the total power. We have checked that the corresponding optical spectra of the orthogonal polarization are very similar to those in Fig. 3. We have also checked that the power in the optical spectra corresponding to the parallel polarization is negligible.

Periodic dynamics is observed for all the values of ν_2. The spectral peaks with highest intensities appear at ν_1 and ν_2. Only one wave mixing peak is visible while the detuning $\nu_1 - \nu_2$ is large [see Fig. 3(a)]. More wave mixing peaks appear as $\nu_1 - \nu_2$ decreases as it is shown in Fig. 3(e). The relative strength of peaks at ν_1 and ν_2 depends on the behaviour of the VCSEL under single optical injection by ML2. The VCSEL emits locked to the optical injection in the orthogonal polarization if $\nu_2 > -26.2$ GHz when subject only to ML2. On the contrary, if $\nu_2 < -26.2$ GHz the VCSEL emits in the parallel direction, no longer being locked to ML2. When both ML1 and ML2 are injecting light into the VCSEL, spectral peaks at ν_1 and ν_2 are similar if $\nu_2 < -26.2$ GHz [see Fig. 3(a)]. On the other hand the peak that appears at ν_2 is the strongest if $\nu_2 > -26.2$ GHz [see Fig. 3(c) and (e)]. In this way the relative strength of peaks at ν_1 and ν_2 changes precisely at the value of ν_2 at which the VCSEL has PS with injection locking under single ML2 injection. Fig. 3(c) is a good example of DIL because the VCSEL is subject to optical injection by both MLs in such a way that stable locking is observed if only light from one of the MLs is injected. The relative strength of peaks at ν_1 and ν_2 changes when DIL appears. We now characterize some parameters related to the optical injection in order to compare with our theoretical results. The value of the injection efficiency factor, η, is estimated by using only the injection given by ML2 in the following way. First, we measure the power at port 3 of the circulator when the slave VCSEL is on and ML2 is off: $P_{vcsel} = 242.8\ \mu W$. We repeat the measurement but when the slave VCSEL is off and ML2 is on: $P_{ml2} = 77.2\ \mu W$. The detected power at port 3

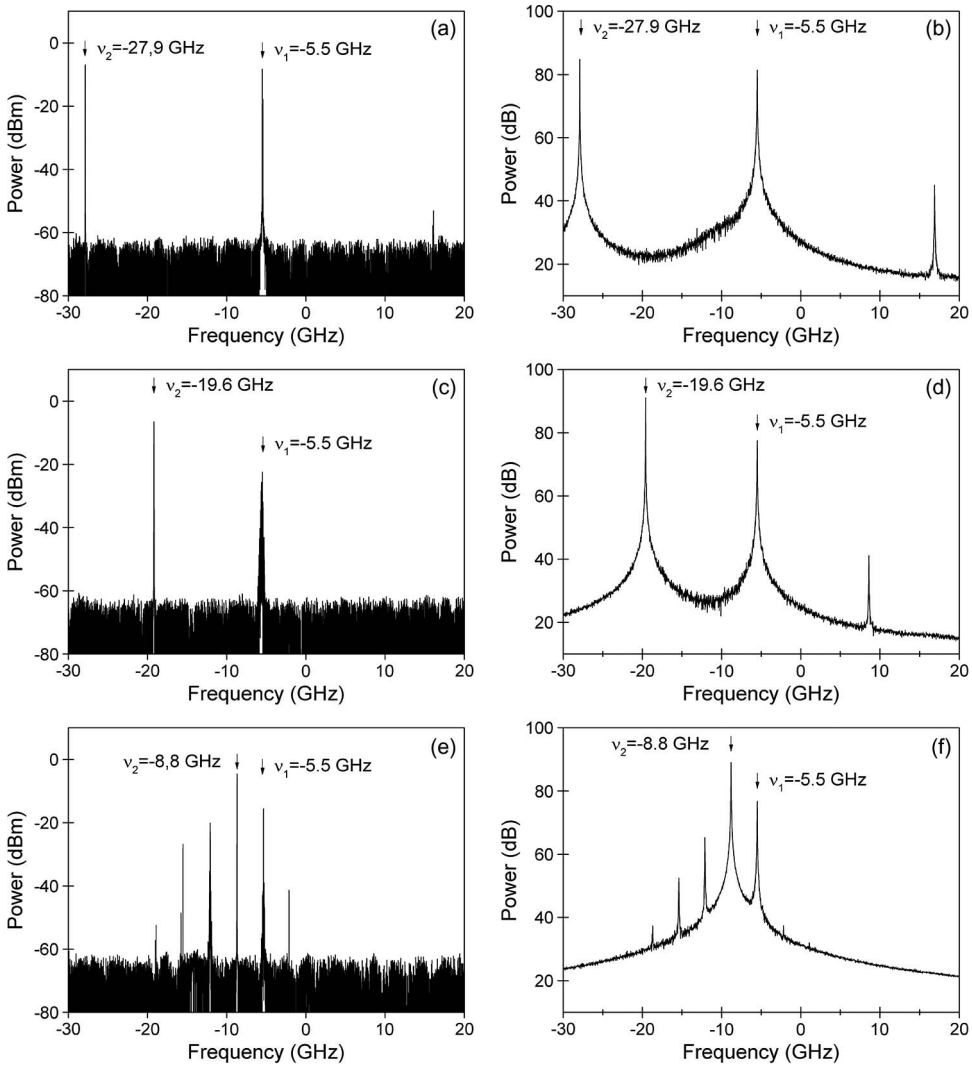

Fig. 3. (Left) Experimental and (right) theoretical optical spectrum with I = 4 mA, $\nu_1 = -5.5$ GHz and (a) and (b) $\nu_2 = -27.9$ GHz, (c) and (d) $\nu_2 = -19.6$ GHz, and (e) and (f) $\nu_2 = -8.8$ GHz.

is $c|\vec{E}_{obs}|^2$, where c is a proportionality constant. Using (8), we would obtain that $P_{vcsel} = c(|E_x|^2 + |E_y|^2)$ and that $P_{ml2} = c\eta^2 R E_{inj,2}^2$. Using these expressions, we obtain

$$\eta = \sqrt{\frac{P_{ml2}}{P_{vcsel}} \frac{|E_x|^2 + |E_y|^2}{R E_{inj,2}^2}} \tag{9}$$

The integration of (1)–(6) with $E_{inj,1} = E_{inj,2} = 0$ gives $|E_x|^2 + |E_y|^2 = 2.4$. The value of $E_{inj,2}$ can be obtained as the value in which we obtain locking at a negative value of ν_2, -26.2 GHz, similar to the experimentally observed when the VCSEL is subject to single optical injection by ML2. The integration of (1)–(6) with $E_{inj,1} = 0$ gives this locking at $E_{inj,2} = 7.5$. Substitution of these values in (9) gives $\eta = 0.116$. The ratio of the injected powers, $E_{inj,1}^2/E_{inj,2}^2 = \mathrm{P_{ML1}}/\mathrm{P_{ML2}}$ can be used to obtain $E_{inj,1} = 2.65$. Finally, values of $\beta_1 (= 0.015\ \mathrm{ns}^{-1})$ and $\beta_2 (= 0.0015\ \mathrm{ns}^{-1})$ have been chosen to obtain linewidths of 4.77 MHz and 0.48 MHz for ML1 and ML2, respectively.

The theoretical spectra corresponding to the experimental cases are shown in the right column of Fig. 3. These spectra have been obtained by integrating (1)–(6) with an integration time

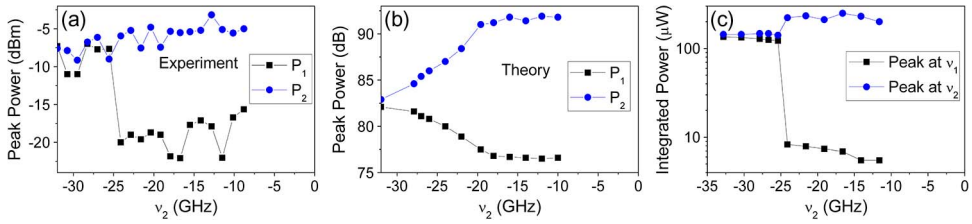

Fig. 4. (a) Experimental and (b) theoretical magnitudes of peaks in optical spectrum at ν_1 and ν_2 as a function of ν_2. (c) experimental integrated power around ν_1 and ν_2 as a function of ν_2. In this figure, I = 4 mA, $\nu_1 = -5.5$ GHz.

step of 0.01 ps to obtain E_x and E_y. The substitution of these values in (8) permits the calculation of the optical spectrum corresponding to $\vec{E}_{obs}(t)$, that is the one that should be compared with the experimental spectrum. Our spectra are obtained by using a 5 ps sampling time and an average over 10 temporal windows of 40.96 ns duration after a transient of 80 ns. The duration of the temporal window has been chosen to obtain a separation between consecutive points in the spectrum of 24.4 MHz, which is a value of the order of the resolution of our optical spectrum analyzer. The position of the peaks and their relative values are similar to those found experimentally. This good agreement between theory and experiment will be the basis of the discussion on the physics behind our results that will be done in the following section.

We now analyze in Fig. 4 the magnitudes of the peaks in the optical spectrum at ν_1 and ν_2, P_1 and P_2, respectively, as a function of ν_2 when $\nu_2 < 0$. Good agreement is observed between the experimental and theoretical results shown in Fig. 4(a) and (b), respectively. Fig. 4(a) and (b) shows that P_1 and P_2 are similar when $\nu_2 < -25$ GHz, a value that is very close to the value, -26.2 GHz, at which the locking under single injection by ML2 appears. When there is DIL ($\nu_2 > -25$ GHz) P_2 becomes clearly larger than P_1, typically 14 dB, in agreement with the discussion of Fig. 3. Fluctuations observed in Fig. 4(a) are typical of the magnitudes of narrow peaks when measured in a high-resolution OSA, possibly due to optical feedback effects. Integrated power measured around each peak does not have those large fluctuations and complements the results of Fig. 4(a). We have done this measurement using the integration function of our OSA with a 5 GHz span and our results are shown in Fig. 4(c). A transition from similar values of the integrated powers to a situation where the integrated power around the peak at ν_2 has the largest value appears close again to $\nu_2 = -25$ GHz.

Fig. 5 shows the results obtained when the frequency of ML1 is kept fixed to a different value ($\nu_1 = 3.75$ GHz) while ν_2 is changed. Similarly to Fig. 3, P_{ML1} and ν_1 are such that there is injection-locked PS under single optical injection. However, in contrast with Fig. 3 in this set of measurements, $\nu_1 > 0$ and $\nu_2 > \nu_1$. Similar trends to those shown in Fig. 3 are observed. The spectral peaks with highest intensities appear again at ν_1 and ν_2. Fig. 5 shows that there are more wave mixing peaks when $\nu_2 - \nu_1$ is small. Fig. 5(a) and (b) illustrate a situation of DIL and similarly to Fig. 3(c)–(f) the strength of the peak at ν_2 is clearly larger than that corresponding to the peak at ν_1. DIL dissappears when ν_2 is increased as it is illustrated in Fig. 5(c) and (d). Now, similarly to Fig. 3(a) and (b), the strength of peaks found at ν_1 and ν_2 becomes similar. Under single ML2 injection, experimentally we find that the VCSEL is locked if $\nu_2 < 20.4$ GHz while theoretically locking occurs if $\nu_2 < 21$ GHz. In Fig. 5 the values of ν_2 have been chosen to illustrate, both in experiment and theory, the transition from a situation with DIL [see Fig. 5(a) and (b)] to a situation without it [see Fig. 5(c) and (d)].

Although good qualitative agreement is obtained between theoretical and experimental spectra we also observe some differences. Figs. 3 and 5 show that the experimental linewidth of each individual peak is determined by a Gaussian lineshape while the theoretical linewidth is determined by a Lorentzian lineshape. While the Lorentzian nature of the theoretical spectra is due to the only noise considered in our model, the spontaneous emission noise, other noise sources are present in the experiment that can affect the observed spectra causing their

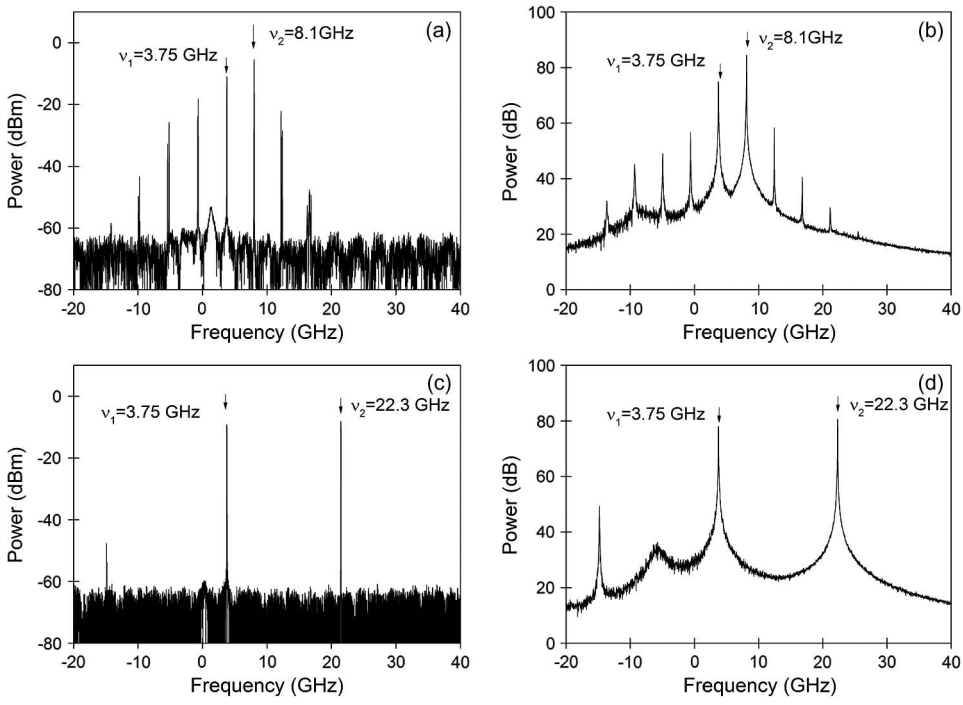

Fig. 5. (Left) Experimental and (right) theoretical optical spectrum with I = 4 mA, $\nu_1 = 3.75$ GHz and (a) and (b) $\nu_2 = 8.1$ GHz, and (c) and (d) $\nu_2 = 22.3$ GHz.

Gaussian shape. Also, experimental wave mixing peaks are larger than the corresponding theoretical ones as it can be seen from comparing Fig. 3(e) and (f) or Fig. 5(a) and (b).

The periodic dynamics observed in Figs. 3 and 5 is of interest for photonic microwave signal generation [8], [22]. RF spectra corresponding to some of the cases analyzed in Figs. 3 and 5 are now shown in Fig. 6. Spectra corresponding to periodic signals are observed in which the first harmonic appears at a frequency value given by $|\nu_2 - \nu_1|$ in agreement with [8] and [22]. Good agreement between theoretical and experimental results is observed. Our results show that the optical injection affects the dynamics of the slave VCSEL [see Fig. 3(e) and (f) and Fig. 5(a) and (b)] in such a way that the observed RF signal is not just due to a beating in the detector of the beam reflected at the VCSEL mirror and the free-running VCSEL beam. Second and higher order harmonics (not shown in Fig. 6) are much weaker than the first one. For instance, in the simulated results of Fig. 6(b) the difference between the first and the second harmonic is 46 dB. Fig. 5(d) also shows that a weak peak appears in the theoretical spectrum near the $|\nu_2 - \nu_1|/2$ frequency that is not observed in the experimental results of Fig. 5(c).

5. Discussion

5.1. Linewidth Evolution in the Transition to Double Injection Locking

In this subsection we analyze the linewidth in the transition to DIL from a theoretical point of view taking into account the influence of the reflected light on the observed behaviour. We consider the transition that occurs for negative frequency detunings, that is the one illustrated in Figs. 3 and 4. Using (8), we separate the observed e-field in two fields, i.e., $\vec{E}_{obs}(t) = \vec{E}_{emit}(t) + \vec{E}_{reflec}(t)$, where $\vec{E}_{emit}(t) = E_x(t)\vec{i} + E_y(t)\vec{j}$ is the e-field emitted by the VCSEL and $\vec{E}_{reflec}(t) = -\eta\sqrt{R}(E_{inj,1}e^{i(\Delta\omega_1 t+\varphi_1(t))} + E_{inj,2}e^{i(\Delta\omega_2 t+\varphi_2(t))})\vec{i}$ is the injected field reflected at the VCSEL mirror. Fig. 7(a) [Fig. 7(c)] shows the optical spectrum corresponding to $\vec{E}_{obs}(t)$, $\vec{E}_{emit}(t)$, and $\vec{E}_{reflec}(t)$ when there is not (there is) DIL. We only show the regions around ν_1 and ν_2 since the relevant

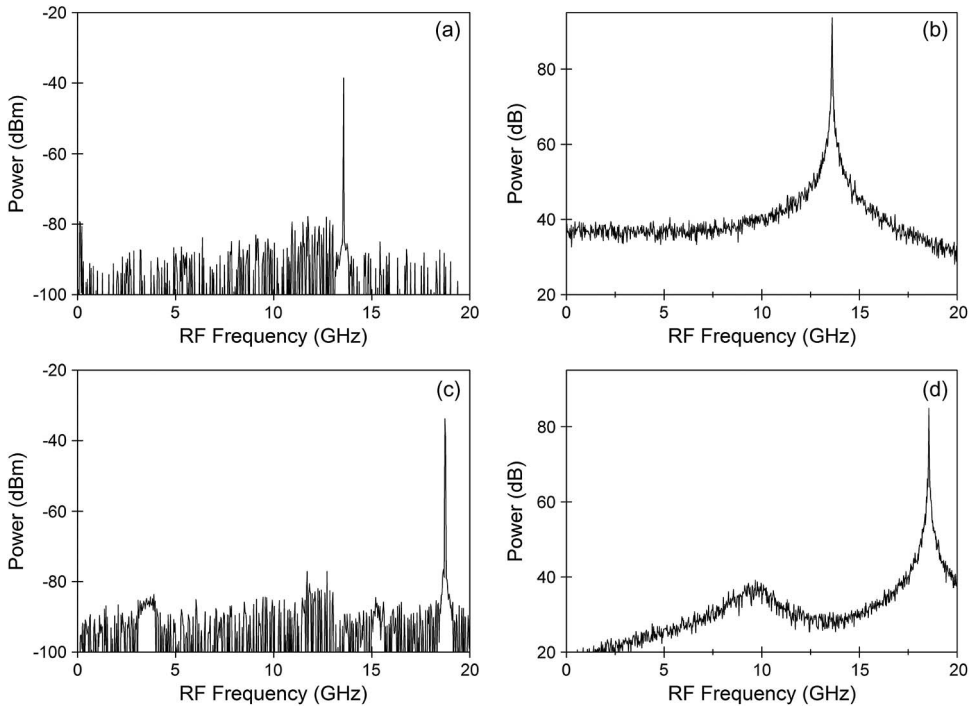

Fig. 6. (Left) Experimental and (right) theoretical RF spectrum with I = 4 mA, (a) and (b) $\nu_1 = -5.5$ GHz, $\nu_2 = -19.1$ GHz, and (c) and (d) $\nu_1 = 3.75$ GHz, $\nu_2 = 22.3$ GHz.

information is contained there. The optical spectra in this figure are obtained with an average of 50 temporal windows of 2.62 μs duration to obtain a separation between consecutive points of 0.38 MHz. This is the reason why the values of the peaks change with respect to those shown in Fig. 3.

Optical spectra corresponding to the reflected field are much smaller than the observed and emitted spectra. The influence of the reflected e-field on the magnitude of the observed spectra in Fig. 7(a) and (c) is small because of the reduced value of η and therefore the observed and emitted spectra are rather similar. The observed spectrum is slightly smaller than the emitted spectrum (the difference is around 1 dB or smaller) since the injected field has a π phase shift upon reflection at the VCSEL mirror. The VCSEL is emitting in both ν_1 and ν_2 frequencies. The VCSEL emits more power at ν_1 when the VCSEL does not lock to the single ML2 injection [see $P_1 = 109.1$ dB in Fig. 7(a)] than when it locks [see $P_1 = 105.3$ dB in Fig. 7(c)]. Also, the VCSEL emits less power at ν_2 when the VCSEL does not lock to the single ML2 injection [see $P_2 = 116.7$ dB in Fig. 7(a)] than when it locks [see $P_2 = 123.6$ dB in Fig. 7(c)]. Therefore when there is (there is not) DIL a significant fraction of the VCSEL power is transferred to the ν_2 (ν_1) frequency, in agreement with our results of Fig. 4.

Fig. 7(a) and (c) shows that the details of the spectra of the light emitted by the VCSEL are similar to those of the reflected spectra. In fact both spectra overlap if they are vertically shifted. Phase fluctuations of the VCSEL are determined by those of the injected light. Fig. 7(b) and (d) shows a zoom of the RF spectrum near its largest peak (that appears at $|\nu_2 - \nu_1|$ frequency) corresponding to the optical spectra shown in Fig. 7(a) and (c), respectively. The magnitude of the RF spectral peak increases when entering in the DIL region: from 115.4 dB to 118.7 dB in the emitted spectrum, and from 114.7 dB to 116.9 dB in the observed spectrum. Again the RF spectrum of the emitted power can be obtained by vertically shifting the reflected RF spectrum. The shape of the emitted RF spectrum is mainly determined by the shape of the reflected RF spectrum. The emitted and reflected RF peak linewidths are very similar. We would not expect a significant change of the RF peak linewidth in the DIL regime since there is no appreciable change

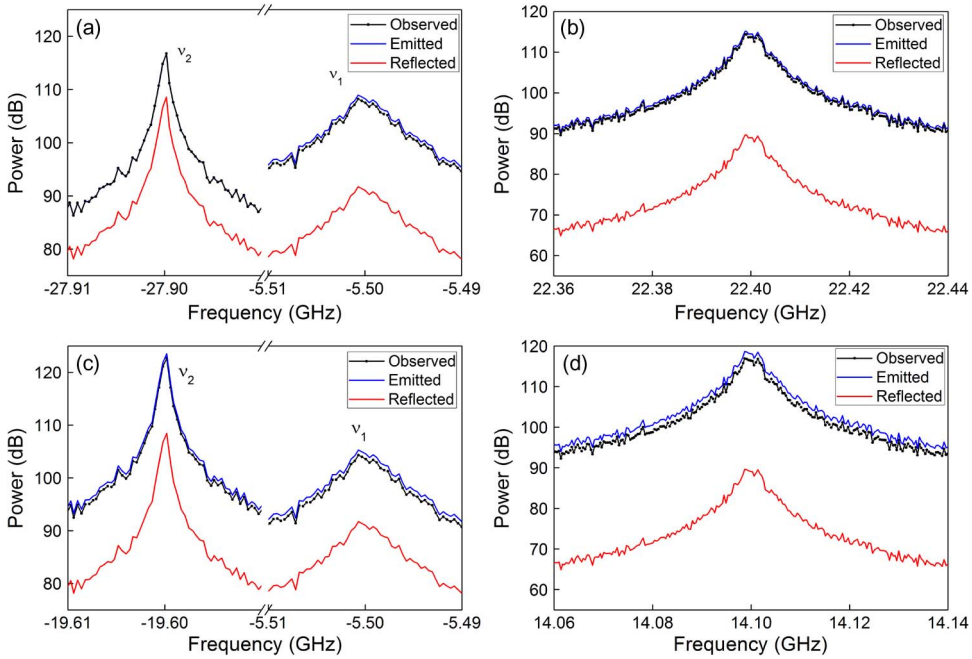

Fig. 7. Theoretical optical spectra for (a) $\nu_2 = -27.9$ GHz and (c) $\nu_2 = -19.6$ GHz. Theoretical RF spectra for (b) $\nu_2 = -27.9$ GHz and (d) $\nu_2 = -19.6$ GHz. Spectra corresponding to the observed, emitted and reflected e-fields are shown with black, blue, and red lines, respectively. In this figure, I = 4 mA, and $\nu_1 = -5.5$ GHz.

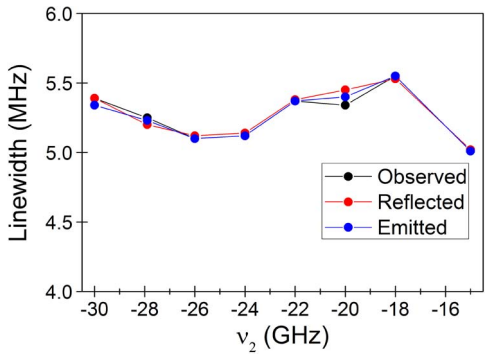

Fig. 8. Calculated observed, reflected, and emitted RF peak linewidth as a function of ν_2. In this figure, I = 4 mA, and $\nu_1 = -5.5$ GHz.

in the reflected RF peak linewidth when entering in this regime. However, a comparison between Fig. 7(b) and 7(d) shows that DIL slightly increases the RF peak linewidth. The 3-dB RF linewidth of the reflected and emitted are similar, 5.2 MHz, in Fig. 7(b). These values are also similar, 5.4 MHz, in Fig. 7(d). These values have been calculated by using a Lorentzian fitting of the spectrum around the peaks. The emitted RF peak linewidth is approximately given by the sum of the linewidths of both optical injections: 5.2 MHz.

In order to determine if there is a significant dependence of the linewidth on the frequency detuning we have calculated the emitted, observed and reflected 3-dB linewidth as a function of ν_2 near the transition to the DIL regime using the same conditions of Fig. 7. Our results are shown in Fig. 8. Linewidth fluctuates around the sum of the linewidths of both optical injections, 5.2 MHz. Although the reflected 3-dB linewidth should be 5.2 MHz, independent of ν_2, some fluctuations inherent to the numerical computation can be seen. Fig. 8 also shows that the

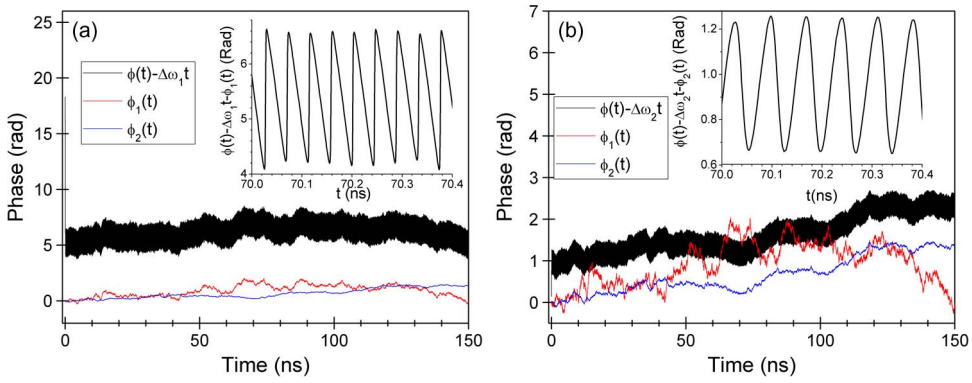

Fig. 9. Optical phase of the light emitted by the slave VCSEL, ML1, and ML2 as a function of time for (a) $\nu_2 = -28.5$ GHz and (b) $\nu_2 = -19.6$ GHz. In this figure, I = 4 mA, and $\nu_1 = -5.5$ GHz.

values of the emitted and observed linewidths are given by those corresponding to the reflected linewidth. Also, Fig. 8 shows that there is no significant variation of the observed nor the emitted linewidth when entering the DIL region ($\nu_2 > -26.2$ GHz).

In our results the linewidth is constant and is given by the sum of the linewidths of both optical injections. The linewidth does not change because the linewidths of the peaks that appear in the optical spectrum at ν_1 and ν_2 are given by the linewidths of ML1 and ML2, respectively. Using the high frequency resolution of Fig. 7, we obtain that in Fig. 3, the linewidths of the peaks at ν_1 andν_2 are 4.8 MHz and 0.5 MHz, respectively, very close to the linewidths of ML1 and ML2. We have checked that this situation also holds for all the other cases considered in this work (see Figs. 5, 7, and 8).

5.2. Optical Phase Evolution in the Transition to Double Injection Locking

In this subsection, we focus on the time evolution of the optical phases for the cases analyzed in Fig. 7. If we write $E_x(t) = A(t)\exp(i\phi(t))$ we can compare the optical phase of the light emitted by the SL to the optical phases of ML1 and ML2, $\phi_1(t)$ and $\phi_2(t)$. We plot in Fig. 9(a) the evolution of $\phi(t) - \Delta\omega_1 t$, $\phi_1(t)$ and $\phi_2(t)$ for the case analyzed in Fig. 7(a). The evolution of the envelope of $\phi(t) - \Delta\omega_1 t$ is similar to $\phi_1(t)$. $\phi(t) - \Delta\omega_1 t$ has rapid oscillations of frequency $|\nu_2 - \nu_1|$. These oscillations can be seen in the inset of Fig. 9(a) in which a zoom of $\phi(t) - \Delta\omega_1 t - \phi_1(t)$ has been plotted as a function of t. The evolution of $\phi(t) - \Delta\omega_1 t - \phi_1(t)$ at any time is very similar to that shown in the zoom, so $\phi(t) - \Delta\omega_1 t - \phi_1(t) = f_1(t)$ where $f_1(t)$ is a periodic function with a $|\nu_2 - \nu_1|$ frequency. Therefore when we are out of the DIL regime the SL is locked to ML1 in the following sense, $\phi(t) = \Delta\omega_1 t + \phi_1(t) + f_1(t)$ where $f_1(t)$ is a periodic function with a $|\nu_2 - \nu_1|^{-1}$ period. The situation is the opposite when the system is in the DIL region, as it can be seen in Fig. 9(b). We now plot $\phi(t) - \Delta\omega_2 t$, $\phi_1(t)$ and $\phi_2(t)$ for the case of Fig. 7(b). The evolution of the envelope of $\phi(t) - \Delta\omega_2 t$ is now similar to $\phi_2(t)$. $\phi(t) - \Delta\omega_2 t$ has also rapid oscillations of frequency $|\nu_2 - \nu_1|$. These oscillations can be seen in the inset of Fig. 9(b) in which a zoom of $\phi(t) - \Delta\omega_2 t - \phi_2(t)$ has been included. Again the evolution of $\phi(t) - \Delta\omega_2 t - \phi_2(t)$ at any time is very similar to that shown in the zoom, therefore, $\phi(t) - \Delta\omega_2 t - \phi_2(t) = f_2(t)$ where $f_2(t)$ is a periodic function with a $|\nu_2 - \nu_1|$ frequency. Therefore, when we are in the DIL regime the slave VCSEL is locked to ML2 in the following sense: $\phi(t) = \Delta\omega_2 t + \phi_2(t) + f_2(t)$ where $f_2(t)$ is a periodic function with a $|\nu_2 - \nu_1|^{-1}$ period. $f_2(t)$ has different average and amplitude values to those of $f_1(t)$ as it can be seen by comparing the insets of Fig. 9.

6. Summary and Conclusion

In this paper we have made an experimental and a theoretical study of the photonic microwave generation using a 1550 nm single transverse mode VCSEL subject to two-frequency orthogonal optical injection. We have focused on the transition to a situation, i.e., the double injection

locking, in which the VCSEL is subject to optical injection by two master lasers in such a way that stable locking is also observed if only light from one of the master lasers is injected. In this situation the frequency of the generated microwave signal corresponds to the frequency difference between both master lasers. We have extended previous existing models to include the effect of the injected light reflected at the VCSEL's mirror and to take into account phase fluctuations in both master lasers. Good agreement is found between experimental and theoretical results obtained using the model with the extracted parameters of our VCSEL. In this way the linewidth has been analyzed from a theoretical point of view. We have studied if a significant reduction of the linewidth is achieved in the double injection locking regime and we have observed no significant reduction with respect both master lasers because the linewidth is mainly determined by the phase fluctuations of the two master lasers. We have obtained that the linewidths of the peaks that appear in the optical spectrum at ν_1 and ν_2 are given by the linewidths of ML1 and ML2, respectively. In this way, the RF linewidth is constant and is given by the sum of the linewidths of both optical injections. Our results concerning the linewidth are only theoretical and an experimental confirmation would be desirable. Further investigations are needed to know if our results also apply to other cases of double injection locking like those considered in [8]. An advantage of single-beam optical injection is that the microwave frequency can be stabilized through various microwave locking techniques applied to the slave laser [36], [37]. These techniques can not be directly applied if the microwave is instead generated by heterodyning two independent lasers [36]. It could be possible that, as for single optical injection, the microwave signal obtained under double optical injection could be stabilized through locking techniques applied to the slave laser. This would be an advantage over the optical mixing method.

Acknowledgement

A. Quirce acknowledges the Fonds Wetenschappelijk Onderzoek for her post-doctoral fellowship.

References

[1] J. Ohtsubo, *Semiconductor Lasers: Stability, Instability, and Chaos*. New York, NY, USA: Springer-Verlag, 2007, ser. Springer Series in Optical Sciences.
[2] D. Parekh *et al.*, "Long distance single-mode fiber transmission of multimode VCSELs by injection locking," *Opt. Exp.*, vol. 18, no. 20, pp. 20 552–20 557, Sep. 2010.
[3] A. J. Seeds and K. J. Williams, "Microwave photonics," *J. Lightw. Technol.*, vol. 24, no. 3, pp. 4628–4641, Feb. 2006.
[4] J. Yao, "Microwave photonics," *J. Lightw. Technol.*, vol. 27, no. 3, pp. 314–335, 2009.
[5] J. Capmany, G. Li, C. Lim, and J. Yao, "Microwave photonics: Current challenges towards widespread application," *Opt. Exp.*, vol. 21, no. 19, pp. 22 862–22 867, Sep. 2013.
[6] X. Q. Qi and J. M. Liu, "Photonic microwave applications of the dynamics of semiconductor lasers," *IEEE J. Sel. Topics Quantum Electron.*, vol. 17, no. 5, pp. 1198–1211, Sep./Oct. 2011.
[7] L. Goldberg, H. F. Taylor, J. F. Weller, and D. M. Bloom, "Microwave signal generation with injection locked laser diodes," *Electron. Lett.*, vol. 19, no. 13, pp. 491–493, Jun. 1983.
[8] Y. S. Juan and F. Y. Lin, "Photonic generation of broadly tunable microwave signals utilizing a dual-beam optically injected semiconductor laser," *IEEE Photonics J.*, vol. 3, no. 4, pp. 644–650, Aug. 2011.
[9] J. P. Zhuang and S. C. Chan, "Tunable microwave generation using optically injected semiconductor laser dynamics with optical feedback stabilization," *Opt. Lett.*, vol. 38, no. 3, pp. 344–346, Feb. 2013.
[10] S. C. Chan, "Analysis of an optically injected semiconductor laser for microwave generation," *IEEE J. Quantum Electron.*, vol. 46, no. 3, pp. 421–428, Mar. 2010.
[11] S. C. Chan, S. K. Hwang, and J. M. Liu, "Radio-over-fiber AM-to-FM upconversion using an optically injected semiconductor laser," *Opt. Lett.*, vol. 31, no. 15, pp. 2254–2256, Aug. 2006.
[12] T. B. Simpson and F. Doft, "Double-locked laser diode for microwave photonics applications," *IEEE Photon. Technol. Lett.*, vol. 11, no. 11, pp. 1746–1748, Nov. 1999.
[13] T. B. Simpson, J. M. Liu, M. Almulla, N. G. Usechak, and V. Kovanis, "Linewidth sharpening via polarization-rotated feedback in optically injected semiconductor laser oscillators," *IEEE J. Sel. Topics Quantum Electron.*, vol. 19, no. 4, Jul./Aug. 2013, Art. ID. 6415240.
[14] C. Cui, S. C. Chan, and J. M. Liu, "Performance analysis on using period-one oscillation of optically injected semiconductor lasers for radio-over-fiber uplinks," *IEEE J. Quantum Electron.*, vol. 48, no. 14, pp. 490–499, Apr. 2012.
[15] Y. H. Hung and S. K. Hwang, "Photonic microwave amplification for radio-over fiber links using period one nonlinear dynamics of semiconductor lasers," *Opt. Lett.*, vol. 38, no. 17, pp. 3355–3358, Sep. 2013.

[16] K. H. Lo, S. K. Hwang, and S. Donati, "Optical feedback stabilization of photonic microwave generation using period-one nonlinear dynamics of semiconductor lasers," *Opt. Exp.*, vol. 22, no. 15, pp. 18 648–18 661, Jul. 2014.
[17] T. B. Simpson, J. M. Liu, M. AlMulla, N. G. Usechak, and V. Kovanis, "Tunable oscillations in optically injected semiconductor lasers with reduced sensitivity to perturbations," *J. Lightw. Technol.*, vol. 32, no. 20, pp. 3749–3758, Oct. 2014.
[18] Y. C. Chen, Y. S. Juan, and F. Y. Lin, "High-frequency microwave signal generation in a semiconductor laser under double injection locking," in *Proc. SPIE*, 2011, vol. 7936, Art. ID. 793609.
[19] X. Q. Qi and J. M. Liu, "Dynamics scenarios of dual-beam optically injected semiconductor lasers," *IEEE J. Quantum Electron.*, vol. 47, no. 6, pp. 762–769, Jun. 2011.
[20] H. Y. Liao, J. M. Liu, and F. Y. Lin, "Dynamical characteristics of a dual-beam optically injected semiconductor laser," *IEEE J. Sel. Topics Quantum Electron.*, vol. 19, no. 4, Jul./Aug. 2013, Art. ID. 6395800.
[21] M. AlMulla, X. Q. Qi, and J. M. Liu, "Dynamic maps and scenario transitions for a semiconductor laser subject to dual-beam optical injection," *IEEE J. Sel. Topics Quantum Electron.*, vol. 19, no. 4, Jul./Aug. 2013, Art. ID. 1501108.
[22] A. Quirce and A. Valle, "High-frequency microwave signal generation using multi-transverse mode VCSELs subject to two-frequency optical injection," *Opt. Exp.*, vol. 20, no. 12, pp. 13 390–13 401, Jun. 2012.
[23] A. Quirce, A. Valle, H. Lin, D. W. Pierce, and Y. Zhang, "Photonic generation of high-frequency microwave signals utilizing a multi-transverse-mode vertical-cavity surface-emitting laser subject to two-frequency orthogonal optical injection," *J. Opt. Soc. Amer. B, Opt. Phys.*, vol. 29, no. 12, pp. 3259–3270, Dec. 2012.
[24] R. Michalzik, *VCSELs: Fundamentals, Technology, and Applications of Vertical-Cavity Surface-Emitting Lasers*. Berlin, Germany: Springer-Verlag, 2012
[25] F. Koyama, "Recent advances of VCSEL photonics," *J. Lightw. Technol.*, vol. 24, no. 12, pp. 4502–4513, Dec. 2006.
[26] Z. G. Pan *et al.*, "Optical injection induced polarization bistability in vertical-cavity surface-emitting lasers," *Appl. Phys. Lett.*, vol. 63, no. 22, pp. 2999–3001, Nov. 1993.
[27] J. Buesa, I. Gatare, K. Panajotov, H. Thienpont, and M. Sciamanna, "Mapping of the dynamics induced by orthogonal optical injection in vertical-cavity surface-emitting lasers," *IEEE J. Quantum Electron.*, vol. 42, no. 2, pp. 198–207, Feb. 2006.
[28] K. Panajotov, I. Gatare, A. Valle, H. Thienpont, and M. Sciamanna, "Polarization- and transverse-mode dynamics in optically injected and gain-switched vertical-cavity surface-emitting lasers," *IEEE J. Quantum Electron.*, vol. 45, no. 11, pp. 1473–1481, Nov. 2009.
[29] P. Pérez, A. Valle, and L. Pesquera, "Measurement of the intrinsic parameters of single-mode VCSELs," *J. Lightw. Technol.*, vol. 32, no. 8, pp. 1601–1607, Apr. 2014.
[30] P. Pérez, A. Valle, and L. Pesquera, "Polarization-resolved characterization of long-wavelength VCSEL parameters," *J. Opt. Soc. Amer. B, Opt. Phys.*, vol. 31, no. 11, pp. 2574–2580, Nov. 2014.
[31] W. Yang, P. Guo, D. Parekh, and C. J. Chang-Hasnain, "Reflection-mode optical injection locking," *Opt. Exp.*, vol. 18, no. 20, pp. 20 887–20 893, Sep. 2010.
[32] P. Guo *et al.*, "Optical phase modulation based on directly modulated reflection-mode OIL-VCSEL," *Opt. Exp.*, vol. 21, no. 19, pp. 22 114–22 123, Sep. 2013.
[33] J. Martin-Regalado, F. Prati, M. San Miguel, and N. B. Abraham, "Polarization properties of vertical-cavity surface-emitting lasers," *IEEE J. Quantum Electron.*, vol. 33, no. 5, pp. 765–783, Apr. 1997.
[34] S. Wieczorek and W. W. Chow, "Bifurcations and chaos in a semiconductor laser with coherent or noisy optical injection," *Opt. Commun.*, vol. 282, no. , pp. 2367–2379, Jun. 2009.
[35] A. Hurtado, A. Quirce, A. Valle, L. Pesquera, and M. J. Adams, "Nonlinear dynamics induced by parallel and orthogonal optical injection in 1550 nm vertical-cavity surface-emitting lasers (VCSELs)," *Opt. Exp.*, vol. 18, no. 9, pp. 9423–9428, Apr. 2010.
[36] S. C. Chan and J. M. Liu, "Frequency modulation on single sideband using controlled dynamics of an optically injected semiconductor laser," *IEEE J. Quantum Electron.*, vol. 42, no. 7, pp. 699–705, Jul. 2006.
[37] S. C. Chan and J. M. Liu, "Tunable narrow-linewidth photonic microwave generation using semiconductor laser dynamics," *IEEE J. Sel. Topics Quantum Electron.*, vol. 10, no. 5, pp. 1025–1032, Sep./Oct. 2004.